A Numerical Approach to Three-Dimensional Dendritic Solidification

Ryo Kobayashi

CONTENTS

We consider pattern formation during the supercooling solidification of a pure material, using a phase field model. The model gives rise to a rich variety of three-dimensional patterns, including very realistic dendritic crystal forms. We show how the strength of anisotropy has a crucial influence on the shape of crystals.

1. INTRODUCTION

Crystal growth is an interesting phenomenon that presents spontaneous pattern formation at macroscopic scales. Dendritic crystals are the most typical examples of such patterns. In this article, we describe one attempt to understand the mechanism of dendritic pattern formation in three dimensions, using a mathematical model and numerical simulations based on it.

There are several types of crystallization: vapor growth, solute growth, melt growth, and so on. In a dilute environment like vapor or solute, crystals are usually bounded by facets. They grow by a process called lateral growth, in which the interface is flat at the molecular level and advances by steps one-molecule high that sweep over it. The growth rate of the crystal is determined by the sweeping velocity of the steps and the frequency of the step-supplying process, such as two-dimensional nucleation or screw dislocation. If supersaturation is not very large, the interfaces are kept macroscopically flat. Once supersaturation becomes larger than some critical value, the crystal presents a complicated form, as in the case of snowflakes [Yokoyama and Kuroda 1990].

1058-6458/94 $0.50 per page

By contrast, the crystallization process in a concentrated environment like melt is usually of a different kind. Macroscopically the crystals are soft-shaped, corresponding to the profile of the diffusion field surrounding them. At the molecular level, the solid-liquid interface is rough and the molecules coming to the interface attach to it immediately and are taken into the solid phase; this is called attaching growth. In this process, the solid-liquid interface is much broader than in lateral growth. Although the process of attaching growth is not understood as clearly as that of lateral growth at the microscopic level, it is easier to treat in macroscopic models. This is because we don't have to consider the transport of molecules along the interface, nor the distribution of the step sources. Therefore the growth rate of crystals can be considered to depend on the supercooling and on the geometric configuration at each point on the interface, making the mathematical modeling easier.

In this article we present a model and numerical simulations of macroscopic pattern formation in the solidification of pure materials. We are especially interested in dendritic crystal growth. This type of growth has been studied in a supercooled melt of succinonitrile [Huang and Glicksman 1981], helium 4 [Franck and Jung 1986], krypton [Bilgram et al. 1988], and in supersaturated solutions of ammonium bromide [Honjo and Sawada 1982; Dougherty et al. 1987; Maurer et al. 1989]. Theoretically, several models have been proposed: a geometric model [Brower et al. 1983], a boundary-layer model [Ben-Jacob et al. 1984], and a fully nonlinear model [Pelcé and Pomeau 1986; Caroli et al. 1986; Barbieri et al. 1986; Ben Amar and Pomeau 1986; Meiron 1986; Kessler et al. 1986]. Numerical simulations were carried out for the fully nonlinear model, and the anisotropy dependence of growth velocity was investigated [Saito et al. 1987]. But this approach based on the fully nonlinear model has been limited to two-dimensional cases. It is important to provide some models to simulate three-dimensional crystal growth, because there are some features of this case that do not arise in any two-dimensional simulation.

What we propose here is a so-called phase field model. It handles motions of interfaces by using the layer dynamics of a certain reaction diffusion system, which enables us to simulate three-dimensional problems. It was introduced as a model of solidification of pure material [Langer 1986; Collins and Levine 1985; Fix 1983] and has been studied to establish the physical and mathematical validities [Caginalp 1986; 1989; 1991; Umantsev and Roitburd 1988; Fife and Penrose 1990]. Elsewhere [Kobayashi 1987; 1991; 1993] I have introduced another type of phase field model, and showed that the formation of dendritic crystals can be simulated in two dimensions. Moreover, the formation of three-dimensional dendrites is simulated in [Kobayashi 1991] (videotape part) and [Kobayashi 1992], to my knowledge for the first time. The purpose of this article is to extend the results of [Kobayashi 1991; 1992] to the morphological aspect of the crystals.

In our model, the shape of the crystal is expressed by a function called the phase field. In this paper we use as the phase field the ordering parameter $p(\boldsymbol{r}, t)$ at the position $\boldsymbol{r}$ and the time t. The liquid phase is indicated by $p = 0$, the solid phase by $p = 1$, and the solid-liquid interface by a steep transition layer connecting the values $p = 0$ and 1 (see Figure 1 for a two-dimensional example). The thickness of the transition layer is small—of order ε, where ε is a small positive parameter explained shortly. We will refer to this thin layer as "the *interface*", using the italics to distinguish it from the real solid-liquid interface of the crystal we are modeling (this is discussed in more detailed later).

Any type of phase field model includes a small parameter ε representing the order of magnitude of the *interface* thickness. In attaching growth, this thickness is not negligible in comparison with molecular dimensions, but it is very small compared with the macroscopic characteristic size of the phenomena we are interested in. Thus we have to handle very different length scales if we take

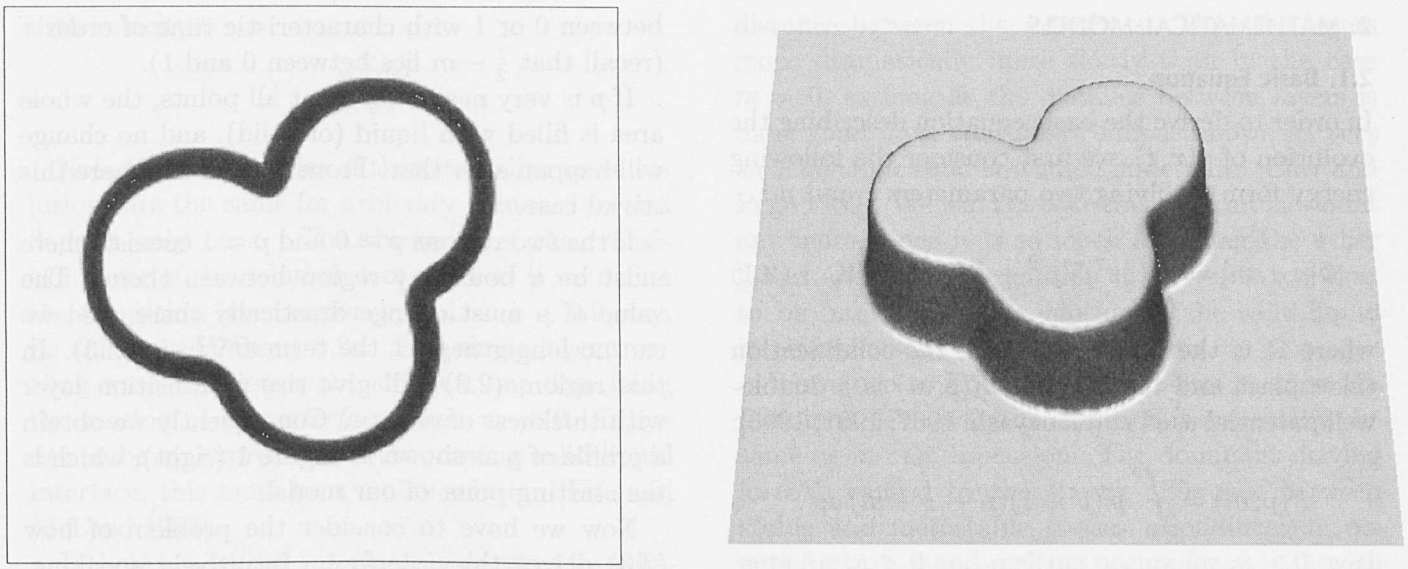

FIGURE 1. An example of the phase field $p(\boldsymbol{r}, t)$ in the two-dimensional space. On the left, the dark region corresponds to the solid-liquid interface. On the right, the graph of the function viewed in perspective: the higher region indicates the solid phase, and the lower region the liquid phase.

ε as the true thickness of the real interface. As long as we consider the model theoretically, there's no problem making ε small: this in fact makes things easier, for example, in asymptotic expansions [Caginalp 1989; 1991]. We can even take the limit $\varepsilon \downarrow 0$.

However, from the simulation point of view, we have a serious problem if ε is very small, for the computational cell size should be of the same order as ε at its largest in order to express and drive our *interface*. Thus, simulating macroscopic pattern formation with very small ε (corresponding to the thickness of the real interface) would require an ideal computer with extremely large memory and extremely high speed. This is impractical in dimensions greater than one.

Thus we take the following standpoint. Imagine that we observe the interface with a microscope whose resolution is of an order ε that is not so fine. This means that we observe some physical quantity $f(\boldsymbol{r})$ as $f * w_\varepsilon(\boldsymbol{r})$, where $w_\varepsilon(\boldsymbol{r})$ is some positive function supported in the ε-neighborhood of the origin and having total mass one. If we take for $f(\boldsymbol{r})$ the characteristic function of the solid region (the thickness of the interface being zero or realistically thin), the observed quantity will be similar to the function that we use as a phase field in our model. Thus we regard our computer as a not-very-good microscope, and interpret the simulation (with ε rather larger than the thickness of the real interface) as an attempt to approximate the motion of the real interface by the motion of the much broader *interface*. In particular, ε is not a physically determined parameter, but rather a parameter determined (more or less arbitrarily) by the simulator's intention and resources. We will return to this point in Section 4.

In Section 2 we introduce the phase field model and show that it falls within the reaction diffusion equation framework. Then we make the model anisotropic in a certain way. In Section 3 we present the three-dimensional simulations of the solidification in supercooled melt, and study in particular the effect of anisotropy on the growth process and on the crystal shapes. In Section 4 we make some additional comments about the model, discussing the problems associated with it.

2. MATHEMATICAL MODELS

2.1. Basic Equation

In order to derive the basic equation describing the evolution of $p(\boldsymbol{r}, t)$, we first consider the following energy form involving two parameters ε and m:

$$\Phi[p; \varepsilon, m] = \int_\Omega (\tfrac{1}{2}\varepsilon^2 |\nabla p|^2 + F(p; m))\, dV, \qquad (2.1)$$

where Ω is the region in which the solidification takes place and the function $F(p; m)$ is a double-well potential used in [Kobayashi 1987; 1991; 1993]:

$$F(p; m) = \int_0^p p'(p' - 1)(p' - \tfrac{1}{2} + m)\, dp'.$$

Here $m \in (-\frac{1}{2}, \frac{1}{2})$, which ensures that the potential $F(p; m)$ always has two local minima, at $p = 0$ and $p = 1$. The difference $F(0; m) - F(1; m)$ between the minima is $\frac{1}{6}m$. If $m > 0$, the solid phase ($p = 1$) is stable and the liquid phase ($p = 0$) is metastable, which means the temperature is lower than the equilibrium temperature. If $m < 0$, the liquid phase is stable and the solid is metastable, which means the temperature is higher than that of equilibrium. If $m = 0$, the two minima are identical, and the temperature is that of equilibrium.

The variable p is an ordering parameter and not a conserved quantity. Thus the evolution equation for p can be derived from the gradient formula

$$\tau \frac{\partial p}{\partial t} = -\frac{\delta \Phi}{\delta p}, \qquad (2.2)$$

namely,

$$\tau \frac{\partial p}{\partial t} = \varepsilon^2 \nabla^2 p + p(1 - p)(p - \tfrac{1}{2} + m). \qquad (2.3)$$

This simple reaction diffusion equation is the basic equation for our phase field model.

We give a rough sketch of the behavior of the solution of (2.3). Since the parameter ε is small, we can neglect the laplacian term in (2.3) if p does not change abruptly in space. Then we have ordinary differential equations at each point, and p varies between 0 or 1 with characteristic time of order τ (recall that $\frac{1}{2} - m$ lies between 0 and 1).

If p is very near 0 (or 1) at all points, the whole area is filled with liquid (or solid), and no change will happen after that. From now on we ignore this trivial case.

If the two regions $p \approx 0$ and $p \approx 1$ coexist, there must be a boundary region between them. The value of p must change drastically there, and we can no longer neglect the term $\varepsilon^2 \nabla^2 p$ in (2.3). In this region, (2.3) will give rise a transition layer with thickness of order ε. Consequently we obtain a profile of p as shown in Figure 1 (right), which is the starting point of our model.

Now we have to consider the problem of how (2.3) drives this *interface*. Intuitively speaking, there are three types of driving force, as we will see below.

But first we state the situation more formally. Equation (2.3) has three spatially constant steady-state solutions $p \equiv 0$, $p \equiv 1$ and $p \equiv \frac{1}{2} - m$. The first two solutions are stable, while the last is unstable. It is expected that a traveling wave solution exists connecting these two stable solutions, and this is important for our model. To study this solution, we consider (2.3) in one dimension:

$$\tau \frac{\partial p}{\partial t} = \varepsilon^2 \frac{\partial^2 p}{\partial x^2} + p(1 - p)(p - \tfrac{1}{2} + m). \qquad (2.4)$$

Assume $m > 0$, so the solid phase is stable and the liquid phase is metastable. Now it is easy to see that the nonlinear eigenvalue problem

$$\frac{d^2 U}{d\xi^2} + A\frac{dU}{d\xi} + U(1 - U)(U - \tfrac{1}{2} + m) = 0$$

for $-\infty < \xi < +\infty$, with boundary conditions $U(-\infty) = 1$ and $U(\infty) = 0$, has a solution

$$U(\xi) = \frac{1}{2}\Big(1 - \tanh \frac{\xi}{2\sqrt{2}}\Big)$$

with $A = \sqrt{2}m$. Using this, we can easily see that (2.4) has a traveling wave solution

$$p(x, t) = \frac{1}{2}\Big(1 - \tanh \frac{x - Vt}{2\sqrt{2}\varepsilon}\Big)$$

with velocity

$$V = \frac{\sqrt{2}m\varepsilon}{\tau}.$$

Note that the profiles of these traveling wave solutions are the same for arbitrary values of m and depend only on ε. The thickness of the transition layer of the solution is of order ε: if we define the transition layer region by $0.1 < u < 0.9$, say, its thickness is about 6.2ε. This single-layer traveling wave solution is the simplest one describing the motion of the *interface* when $m \neq 0$. In order to be an expression of the moving solid-liquid interface, this must be a stable solution [Fife and McLeod 1977].

If there are several *interfaces*, separated by a distance significantly greater than their thickness, the profile of $p(x,t)$ in the vicinity of the *interfaces* is almost the same as that of the single layer solution; the velocities in this case are also the same as for a single-layer traveling wave. The situation is the same if the system size is finite. Since m corresponds to an energy difference between two phases, these solutions describe a natural motion, expressing the fact that the stable phase erodes the metastable phase with a velocity proportional to the energy difference. This driving force dominates as long as $m \neq 0$.

Now assume $m = 0$, so the thermodynamic driving force vanishes. In this situation, there are two driving forces. The first, corresponding to surface tension, has no effect in one dimension, so for the one-dimensional equation (2.4) only the second force applies. It is a very weak attractive force between the *interfaces*, of order $e^{-d/\varepsilon}$, where d is the distance between the *interfaces*. Thus the layers move dramatically more slowly than in the case $m \neq 0$, as long as the distance between layers is more than layer thickness. This is known as *very slow dynamics* and is studied in detail in [Carr and Pego 1989]. We will not take this force into account any more, since it is so much less than the other forces and since the motion it causes is too slow to be interpreted as a motion of the solid-liquid interface in solidification phenomena.

We return to Equation (2.3) in two or three dimensions. If $m \neq 0$, the situation is essentially the same as in one dimension. The dominant driving force is caused by the energy difference between stable and metastable phases. Solidification occurs for $m > 0$ and melting occurs for $m < 0$, with rate proportional to $|m|$. To see the surface tension clearly, assume at first that m vanishes, that the dimension is two, and that the initial phase field has the profile indicated on the left in Figure 2, for example. For this phase field, both terms of Φ vanish in both bulk regions. At the *interface*, these terms are positive, which disadvantages the energy. Since, by (2.2), the system evolves in the direction of decreasing Φ, the *interface* will be driven so as to reduce its area, as seen in Figure 2. The thickness of the *interface* is almost fixed according to the value of ε, so the evolution tends to decrease the *interface*'s "length". In three dimensions, it tends to decrease the *interface*'s "area" (roughly speaking, the ratio between volume and thickness). These driving forces correspond to surface tension. If $m \neq 0$, thermodynamic driving force and surface tension coexist, and both of them tend to move the *interface*.

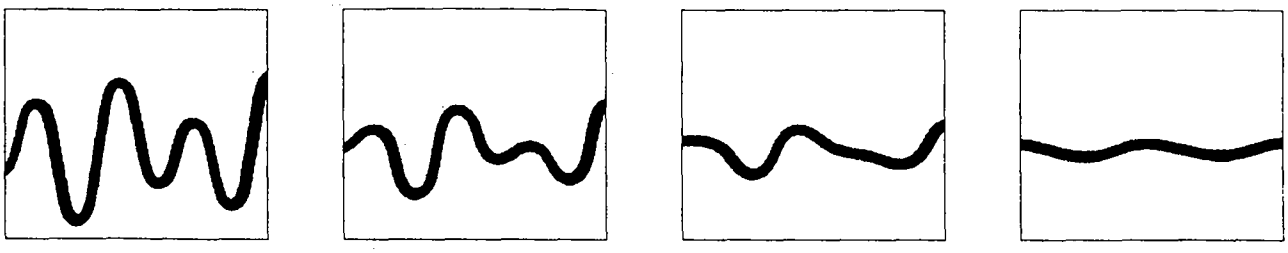

FIGURE 2. Time evolution of the *interface* with $m = 0$ in two dimensions. Time flows from left to right.

In order to make the situation clear, we discuss the sharp interface limit obtained by making ε approach zero. There are different ways to take the limit [Caginalp and Nishiura 1991], depending on what order in ε we take τ and m to be. Here we consider only the case where τ is of order ε^2 and m of order ε. In this way we obtain a limiting equation that includes both surface tension and a thermodynamic driving force. More precisely, with $\tau = a\varepsilon^2$ and $m = f\varepsilon/\sqrt{2}$, we formally obtain the equation

$$aV = f - (N-1)\kappa, \tag{2.5}$$

where V is a normal velocity of the interface (the direction from solid to liquid being taken to be positive), N is the ambient dimension and κ is the mean curvature of the interface (positive if the solid region is convex).

Note that this equation is defined only on the sharp interface itself (that is, on a surface in three dimensions or on a curve in two), while the original equation (2.3) is defined in the ambient region. This is reasonable, because (2.3) contains essential information only in the neighborhood of the *interface*; in the bulk regions it simply says that $0 = 0$, each of its terms being almost zero (since p is essentially identically zero or one in the bulk phases).

If $f = 0$, Equation (2.5) expresses *motion by mean curvature*, and if $f \neq 0$, it describes the motion of the interface caused by the thermodynamic driving force and surface tension. We may consider that the motion of the *interface* expressed by (2.3) approximates the motion of sharp interface given by (2.5). The convergence of (2.3) to (2.5) as $\varepsilon \downarrow 0$ has been rigorously proved [Mottoni and Schatzman 1990].

Here we mention another limit, defined by taking $\tau = a\varepsilon$ and $m = f/\sqrt{2}$. Here the limit equation with $\varepsilon \downarrow 0$ is $aV = f$, and the surface tension term disappears. But in the problem of crystal growth, especially when the shape of crystal destabilizes, forming dendrites, surface tension must be taken into account to suppress the growth of structures with arbitrarily short wavelength. Then usually an equation including the term of order ε is considered instead, such as $aV = f - \varepsilon(N-1)\kappa$. In this equation, ε should be a physical parameter corresponding to capillary length, and therefore cannot be chosen arbitrarily. As stated in the previous section, we prefer to work in a way that frees the parameter ε from such a restriction. This is the case when we take the limit $\tau = a\varepsilon^2$ and $m = f\varepsilon/\sqrt{2}$, the parameter ε being regarded as the width of the *interface*, or as a measure of how well (2.3) approximates (2.5).

Suppose m (or equivalently f) is positive, meaning that the solid phase is stable and the liquid is metastable. There is a radially symmetric solution $p = p(r)$ of (2.3), which means that the one particle of stable phase with radius r_c exists in the surrounding metastable phase. It exists under the balance of the two forces, the first tending to make the particle grow and the second to make it shrink. This solution is unstable since the first force is constant and the second is a decreasing function of the particle radius (a particle with radius greater than r_c will grow and one with radius smaller than r_c will shrink and disappear). We call r_c the *critical nucleation radius*. Of course, its value is very small, so that the facts stated here are about the ideal case in which we can take ε realistically small. In simulations we must give initial particle a radius rather larger than the real critical nucleation radius in order to make the nucleus grow.

In any case, if the particle survives, it keeps growing. Then the problem is what will happen as the particle becomes larger, for example, whether or not some destabilization occurs and patterns appear. From numerical simulations we can easily see that no interesting pattern formation occurs. Even if the initial shape is complicated, the shape of the particle will become simple. Thus (2.3) is not enough in order to simulate a formation of a complicated shape. This is because the complicated shapes arise from the nonuniformity of the thermodynamic driving force along the interface, while m is constant in Equation (2.3).

2.2. Introduction of Anisotropy

Equation (2.3) includes no anisotropy, and crystals have anisotropy. We derive an equation that includes anisotropy by making ε in (2.1) depend on the direction: $\varepsilon = \varepsilon(\boldsymbol{v})$, where $\boldsymbol{v}$ corresponds to the outer normal vector at the interface [Kobayashi 1987; Kobayashi 1993; Kobayashi 1991]. The function $\varepsilon(\boldsymbol{v})$ is assumed to satisfy $\varepsilon(\lambda\boldsymbol{v}) = \varepsilon(\boldsymbol{v})$ for λ positive. The equation becomes

$$\tau\frac{\partial p}{\partial t} = -\nabla\cdot(|\nabla p|^2\varepsilon\frac{\partial\varepsilon}{\partial\boldsymbol{v}}) + \nabla\cdot(\varepsilon^2\nabla p) + p(1-p)(p-\tfrac{1}{2}+m), \quad (2.6)$$

where ε and $\partial\varepsilon/\partial\boldsymbol{v}$ are evaluated at the vector $-\nabla p$. We can also make τ depend on the direction, $\tau(\boldsymbol{v}) = \tau(-\nabla p)$. Thus $\tau(\boldsymbol{v})$ and $\varepsilon(\boldsymbol{v})$ control the anisotropy of the kinetic coefficient and of the surface energy, respectively.

Perhaps this form is the best way to give the anisotropy to the phase field model, since the related sharp interface equation is physically realistic for the two-dimensional case [McFadden et al. 1993; Gurtin].[1] In three-dimensional cases, the sharp interface equation should have the form

$$\beta(\boldsymbol{n})V = f - \Big(\xi(\boldsymbol{n}) + \frac{\partial^2\xi}{\partial s_1^2}(\boldsymbol{n})\Big)\kappa_1 - \Big(\xi(\boldsymbol{n}) + \frac{\partial^2\xi}{\partial s_2^2}(\boldsymbol{n})\Big)\kappa_2 \quad (2.7)$$

as a natural extension of the isotropic equation. In this equation, $\beta(\boldsymbol{n})$ and $\xi(\boldsymbol{n})$ indicate anisotropy in the kinetic coefficient and surface energy, respectively, where $\boldsymbol{n}$ is an outer unit normal vector at the interface. Furthermore, κ_1 and κ_2 are the principal curvatures, and $\partial^2\xi/\partial s_1^2$ and $\partial^2\xi/\partial s_2^2$ are the second derivatives along the directions of the principal curvatures κ_1 and κ_2. It's quite difficult to derive this sharp interface equation from (2.6), and we were not able to do it. But we believe that the correct sharp interface equation is to be derived from (2.6) also in the three-dimensional case.

Here we will introduce a simple alternative to (2.6) in order to decrease the computation time of our numerical simulations. It is given by making m dependent on the direction in (2.3):

$$\tau\frac{\partial p}{\partial t} = \varepsilon^2\nabla^2 p + p(1-p)(p-\tfrac{1}{2}+m(-\nabla p)), \quad (2.8)$$

where τ and ε are constants. We impose the property $m(\lambda\boldsymbol{v}) = m(\boldsymbol{v})$ for arbitrary positive λ, since we want to express the direction dependence by the function $m(\boldsymbol{v})$. The vector $-\nabla p$ indicates the outer normal vector if it is evaluated in the interface region. In the bulk region ∇p is almost zero and therefore we can hardly determine its direction. But there is no problem, because Equation (2.8) works effectively only in the vicinity of the *interface* region and we can take the value of $m(-\nabla p)$ appropriately in the bulk region.

To clarify how (2.8) drives the *interface*, we take the sharp interface limit with $\tau = a\varepsilon^2$ and $m(\boldsymbol{v}) = f\sigma(\boldsymbol{v})\varepsilon/\sqrt{2}$, where $\sigma(\boldsymbol{v})$ is an anisotropy indicator. The resulting equation is

$$aV = f\sigma(\boldsymbol{n}) - (N-1)\kappa. \quad (2.9)$$

This equation means that the sensitivity of the growth rate to the thermodynamic driving force depends on the direction of the interface. To compare (2.9) with (2.7), we introduce direction dependence on a by setting $a = a(\boldsymbol{n})$. Putting $\beta(\boldsymbol{n}) = a(\boldsymbol{n})\sigma(\boldsymbol{n})^{-1}$ and $\xi(\boldsymbol{n}) = \sigma(\boldsymbol{n})^{-1}$, we have

$$\beta(\boldsymbol{n})V = f - \xi(\boldsymbol{n})\kappa_1 - \xi(\boldsymbol{n})\kappa_2.$$

This equation is incomplete since it does not include the second derivative terms of the anisotropy function for the surface energy.

2.3. Model Equation for the Solidification of a Pure Material

To describe the solidification process of pure material, we must make the parameter m in (2.8) should depend on T, the temperature: $m = m(T, \boldsymbol{v})$. And, of course, we must consider the temperature field

[1] I made a mistake in deriving the sharp interface equation from (2.6) in [Kobayashi 1993]: the equation in [McFadden et al. 1993; Gurtin] is correct.

$T(\boldsymbol{r}, t)$ together with the phase field $p(\boldsymbol{r}, t)$. We define the dimensionless temperature T' by $T' = (T - T_e)(L/c)$, where T_e is an equilibrium temperature, L is the latent heat per unit mass and c is the heat capacity per unit mass. The equation governing the evolution of the temperature field is derived from the conservation law of enthalpy:

$$\frac{\partial T'}{\partial t} = D\nabla^2 T' + \frac{\partial p}{\partial t}.$$

Here, for simplicity, the heat capacity and the heat conduction coefficient are assumed to be the same in both phases, and the latent heat does not depend on the temperature at which solidification occurs.

In previous papers [Kobayashi 1987; Kobayashi 1993; Kobayashi 1991; Kobayashi 1992], we defined the dimensionless temperature as $(T - T_{\text{cool}})/(T_e - T_{\text{cool}})$, where T_{cool} is the characteristic cooling temperature, and then we had a dimensionless latent heat K multiplied by the term $\partial p/\partial t$. In this paper, we adopt the above nondimensionalization and no longer use the parameter K. Instead we have another dimensionless parameter Δ (corresponding to K^{-1}) in the initial condition or boundary condition.

Next, we nondimensionalize the space variable by some characteristic crystal size first, and then the time variable to make the diffusion constant equal to one. Thus we arrive at the final model equations for the solidification of a pure material:

$$\tau \frac{\partial p}{\partial t} = \varepsilon^2 \nabla^2 p + p(1-p)(p - \tfrac{1}{2} + m(T, -\nabla p)), \tag{2.10}$$

$$\frac{\partial T}{\partial t} = \nabla^2 T + \frac{\partial p}{\partial t}. \tag{2.11}$$

Note that the primes $'$ are omitted from the notation of the dimensionless temperature.

In order to simulate the evolution of this system of equations, we must specify the form of $m(T, \boldsymbol{v})$. We adopt the arctangent form used in [Kobayashi 1987; 1991; 1993], at the same time making it dependent on the direction. The problem is how to introduce anisotropy in three dimensions. In two dimensions, it is easy to express the anisotropy by some formula such as $1 + \delta \cos 4\theta$, since we can explicitly use the variable θ, the angle between the outer normal vector $\boldsymbol{v}$ at the *interface* and the constant vector $(1, 0)$. In three dimensions, we could still use polar coordinates, but a formula giving a reasonable anisotropy behavior would be somewhat complicated, and the evaluation of inverse trigonometric functions is costly.

We opt for the following formulation. Let $\sigma(\boldsymbol{v})$ be defined as

$$\sigma(\boldsymbol{v}) = 1 - \delta\Big(1 - \frac{|\boldsymbol{v}|_4^4}{|\boldsymbol{v}|_2^4}\Big), \tag{2.12}$$

where $|\boldsymbol{v}|_h = \big(\sum_{i=1}^3 |v_i|^h\big)^{1/h}$ for the three-dimensional vector $\boldsymbol{v} = (v_1, v_2, v_3)$. This form gives a kind of cubic anisotropy (Figure 3). In fact, $\sigma(\boldsymbol{v})$ is invariant under 90° rotations around coordinate axes. Note that $\sigma(\boldsymbol{v}) = 1$ (the maximum value) for $\boldsymbol{v} = (1, 0, 0)$; that $\sigma(\boldsymbol{v}) = 1 - \frac{1}{2}\delta$ for $\boldsymbol{v} = (1, 1, 0)$; and that $\sigma(\boldsymbol{v}) = 1 - \frac{2}{3}\delta$ (the minimum value) for $\boldsymbol{v} = (1, 1, 1)$.

The anisotropy function (2.12) is not derived from a serious physical analysis of molecular array structure or the growth dynamics. It only expresses a rough preference for growth in the directions $(1, 0, 0)$, $(0, 1, 0)$ and $(0, 0, 1)$. The big advantage of this function is that, its computation time is low, since it only involves arithmetic operations.

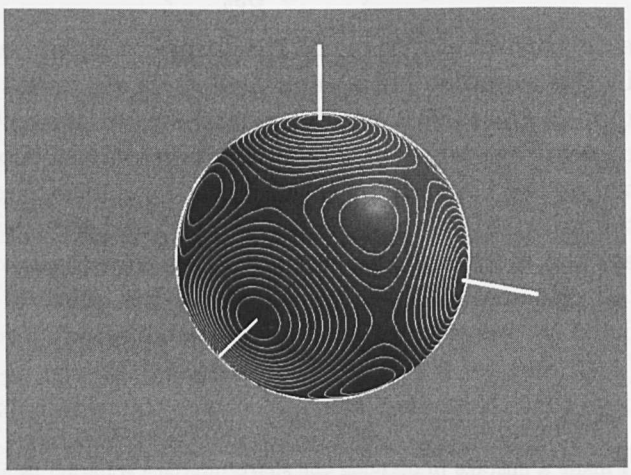

FIGURE 3. Level curves of the anisotropy function $\sigma(\boldsymbol{v})$ on the unit sphere.

We note also that the formula for $\sigma(\boldsymbol{v})$, when restricted to two dimensions, yields the four-mode anisotropy discussed above: $\sigma(\theta) = 1 - \frac{1}{4}\delta(1 - \cos 4\theta)$ for $\theta = \tan^{-1}(v_2/v_1)$.

It may seem unnatural that the anisotropy expressed by $\sigma(\boldsymbol{v})$ is fixed with respect to the coordinate system, but we explain this as follows. Our model describes the growth process of a single crystal. Since the directions of the crystal structure are determined at the nucleation stage and do not change during the growth process, the space coordinates can be chosen so as to coincide with the directions of the cubic crystalline structure.

Using $\sigma(\boldsymbol{v})$, we define $m(T, \boldsymbol{v})$ as

$$m(T, \boldsymbol{v}) = -\frac{\alpha}{\pi} \tan^{-1}(\gamma\sigma(\boldsymbol{v})T).$$

We can introduce fluctuations in the system by adding a small amount of noise to $m(T, \boldsymbol{v})$, which effectively works only in the interface region. The constant $\alpha \in (0, 1)$ is a safety parameter used to assure that $|m(T, \boldsymbol{v})| < \frac{1}{2}$, or $|m(T, \boldsymbol{v}) + \text{noise}| < \frac{1}{2}$ if noise is added to $m(T, \boldsymbol{v})$. If $|T|$ is small enough, we can consider $m(T, \boldsymbol{v})$ linear in T, which means the thermodynamic driving force is proportional to the supercooling at the interface. The parameter γ is a sensitivity parameter by means of which we can control this proportionality constant.

3. SIMULATIONS

In this section we discuss three-dimensional simulations of the solidification of a pure material in supercooled melt using the model equation system (2.10)–(2.11). The vessel is a box with edges parallel to the coordinate axes. As mentioned before, the directions of anisotropy implicit in (2.12) also coincide with the axes.

In all the simulations, the vessel is initially filled with uniformly supercooled melt at dimensionless temperature $-\Delta$, with $\Delta = (T_e - T_{\text{cool}})/(L/c)$, where T_{cool} is the initial temperature of the supercooled melt. Nucleation takes place at the center of one wall and the growth takes place under adiabatic conditions. We do not simulate the process of nucleation, only the growth after nucleation; the nucleus is given as an appropriate initial state for the phase field $p(\boldsymbol{r}, 0)$.

There are two parameters that strongly influence the shape of crystals: the dimensionless supercooling Δ and the strength of anisotropy δ. We have $\Delta = 0.25$ in all the simulations demonstrated here, and we examine how the anisotropy influences the growth process and the crystal forms. The remaining parameters that are common to all the simulations are $\tau = 3.0 \times 10^{-4}$, $\varepsilon = 1.0 \times 10^{-2}$, $\alpha = 0.9$, $\gamma = 40.0$, $\delta x = \delta y = \delta z = 3.0 \times 10^{-2}$, and $\delta t = 1.0 \times 10^{-4}$ (here δx, δy and δz are the space mesh sizes and δt is the time mesh size).

The numerical convergence of the one- and two-dimensional phase field model with respect to space and time mesh sizes was systematically studied in [Wheeler et al. 1993]. In order to perform the three-dimensional simulations using the available computational resources, we chose $\delta x = 3\varepsilon$, which is rather larger than the value $\delta x = \varepsilon$ used in [Wheeler et al. 1993]. Although we could not check numerical convergence for lack of computational power in the three-dimensional case, we are sure that the convergence with the space mesh size and the time mesh size holds. This is because the model equation is simply a reaction-diffusion equation of the usual type, once all the parameters are fixed. However, we have to remember that the convergence for the velocity, radius and temperature of the tip of the principal branch should hold, while we cannot expect the convergence of the sidebranch structure in the strict sense.

In the simulation of the dendritic solidification, the shape of the *interface* is strongly unstable and is subtly affected by noise. Thus convergence will be observed only in the statistic properties of the sidebranch structure.

3.1. The Case of Strong Anisotropy

Figures 4–10 show the results of the simulation for values of δ ranging from 0.2 to 1.0, with the other parameters held fixed. The region size was taken to be $6.0 \times 4.8 \times 4.8$ ($200 \times 120 \times 120$ cells), and

the computations were carried out in a quadrant only, being extended to the other three by reflection in the xy- and xz-planes. All the simulations were carried out by a simple explicit scheme and no special techniques were used. No noise was actively added, although noise caused by the truncation and roundoff is, of course, unavoidable.

$\delta = 0.2$

Figure 4 shows one typical dendritic crystal form, similar to the one seen, for example, in the dendritic growth of succinonitrile in the $(1,1,1)$ direction [Sawada and Inoue]. It has rather dense sidebranch structure, with secondary sidebranches. The most characteristic feature in this growth process is the oscillation in the rate at which the principal branch grows (speed of the tip, as well as its curvature: see the bottom left graph in Figure 4). This kind of oscillation is observed in experiments [Sawada and Inoue]. Here it is rather strong and quickly leads to sidebranches. Thus the distance between the tip of the principal branch and the fully grown sidebranch nearest to it is small compared with the case of nonoscillatory growth shown in Figure 6, for example. The angle between the principal branch and the sidebranches is approximately $\pi/3$, which is shifted from the direction of cubic anisotropy, and almost perpendicular to the contour surface of the temperature field (this is the best direction for sidebranches' growing, due to the effectiveness of the cooling). We also see that, as each sidebranch grows, it splits into three smaller branches. The growth form of each sidebranch is similar to that of the oscillating principal branch seen in two-dimensional simulations [Kobayashi 1993]. The walls of the vessel prevent sidebranches from growing beyond a certain point: the tips of fully grown sidebranches are already blocked by the side walls and cannot grow any more.

$\delta = 0.25$

The crystal form in Figure 5 is very similar to the previous one. The growth rate of principal branch still oscillates, although less (bottom left graph). The principal branch is a bit thicker than in the previous case, while the sidebranch structure is almost the same.

$\delta = 0.3$

Figure 6 shows one of the most typical dendritic growth form. It is observed, for example, in the dendritic growth of succinonitrile to the $(1,0,0)$ direction [Huang and Glicksman 1981]. The shape of the principal branch's tip is approximately a paraboloid of revolution. Its axisymmetry is first broken near the tip into a fourfold fin-like structure, considered to be a direct result of the cubic anisotropy. The oscillation of the growth speed of the principal branch triggered by initial nucleation stage is rapidly damped, and oscillation is no longer observed in the steady growth stage (bottom left graph). Although oscillation is not present to create sidebranches, they nevertheless arise: sidebranch instability takes place on the surface of the fins and the fluctuations with characteristic wavelength are destabilized. Since this instability process takes longer than the oscillatory mechanism, fully developed sidebranches are seen only near the base. For the same reason, the principal branch is thicker than in the preceding cases. Once the sidebranches are created, they grow and ramify as before. Sidebranches compete with each other through the temperature field, and come out as winners or losers. This is also seen in physical experiments.

$\delta = 0.4$

In Figure 7, sidebranch instability still occurs and the sidebranches grow, but only near the base of the principal branch. The destabilization rate is less than in the previous case.

$\delta = 0.5$

In Figure 8, sidebranch instability is even weaker; sidebranches are smaller and the principal branch is thicker. Qualitatively, the crystal form is very similar to the preceding one.

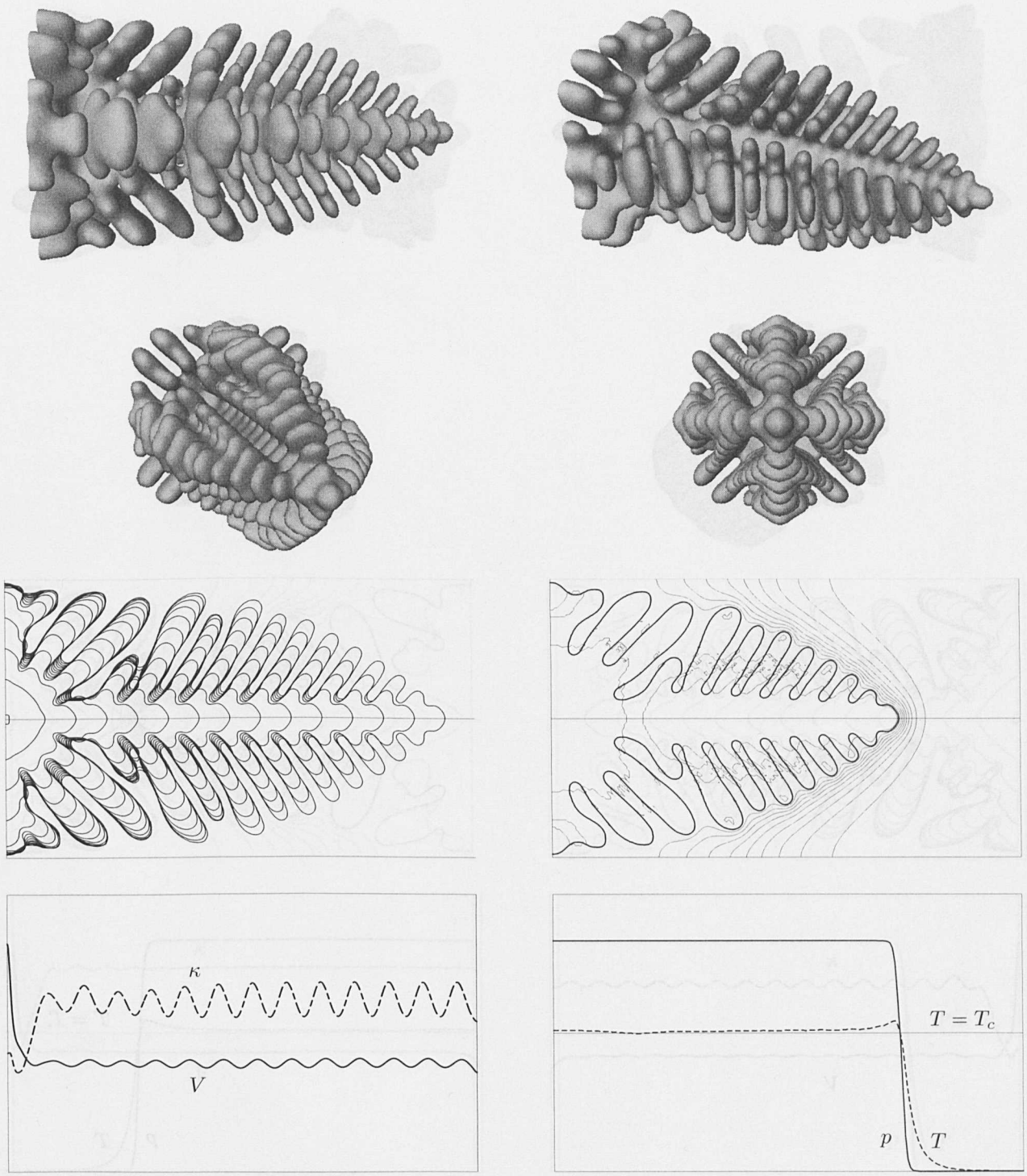

FIGURE 4. Simulation for $\delta = 0.2$. Top two rows: views of the computed crystal. Third row, left: sections of the crystal at successive times; the lower half shows the contour $p = \frac{1}{2}$ of the phase field along the xy-plane, and the upper half the same contour along the xz-plane. Third row, right: for a fixed t, the contour $p = \frac{1}{2}$ and several constant-temperature contours, the innermost being $T = T_c$, the equilibrium temperature. Bottom row, right: for the same t, the graph of p and T along the x-axis. Bottom row, left: graph of the velocity V and mean curvature κ of the tip of the principal branch as a function of time.

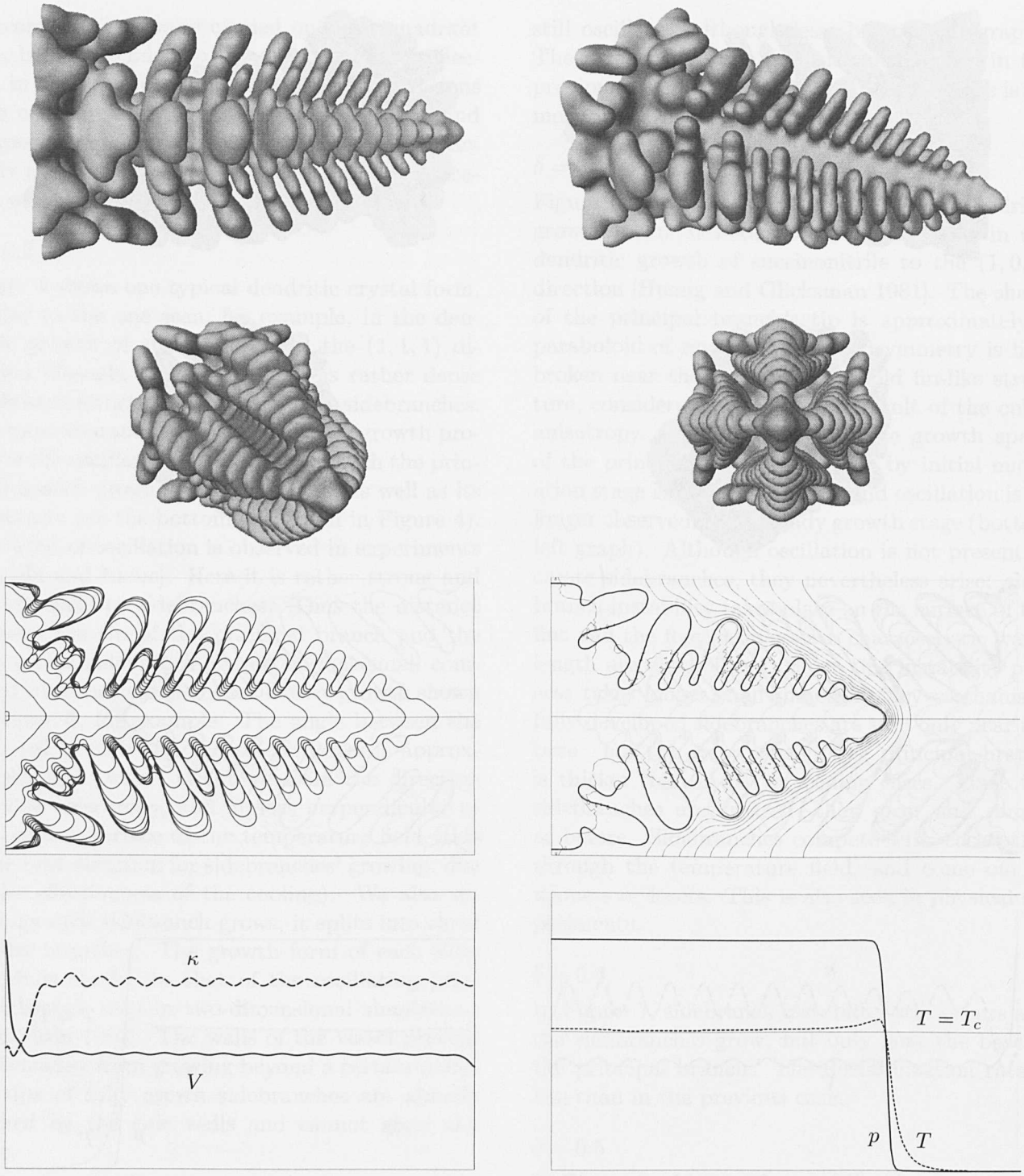

FIGURE 5. Simulation for $\delta = 0.25$. The arrangement is the same as in Figure 4.

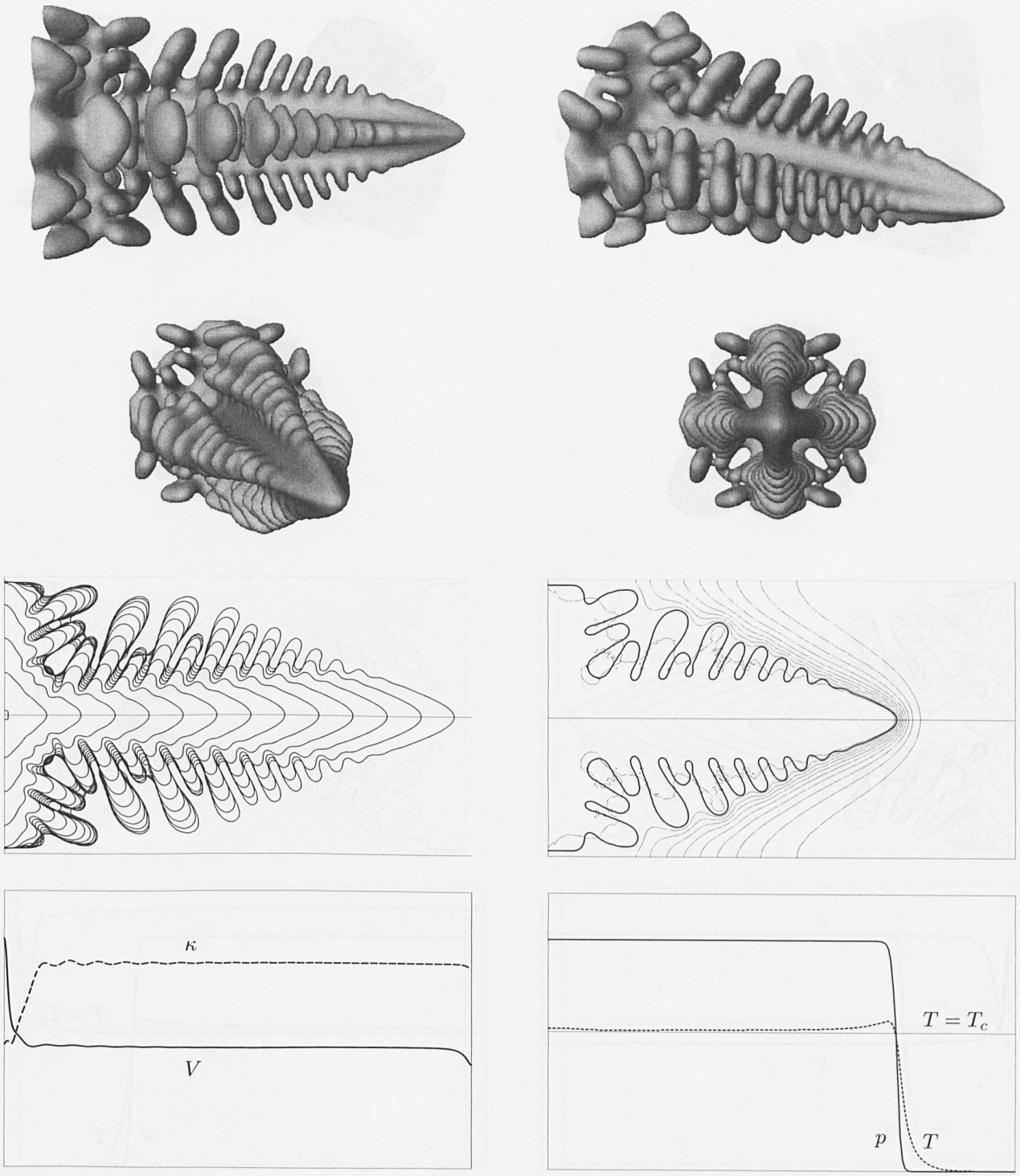

FIGURE 6. Simulation for $\delta = 0.3$. The arrangement is the same as in Figure 4.

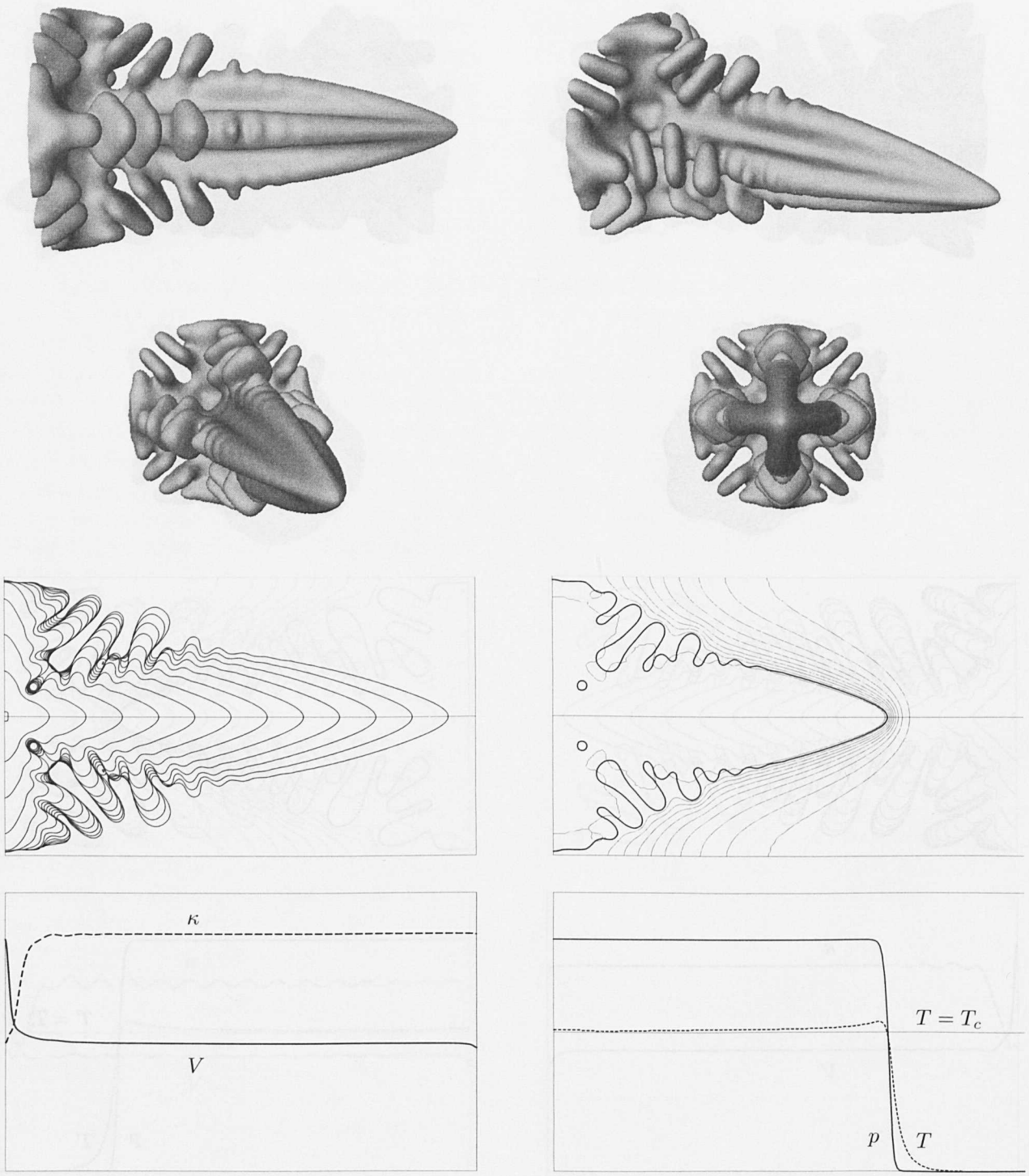

FIGURE 7. Simulation for $\delta = 0.4$. The arrangement is the same as in Figure 4.

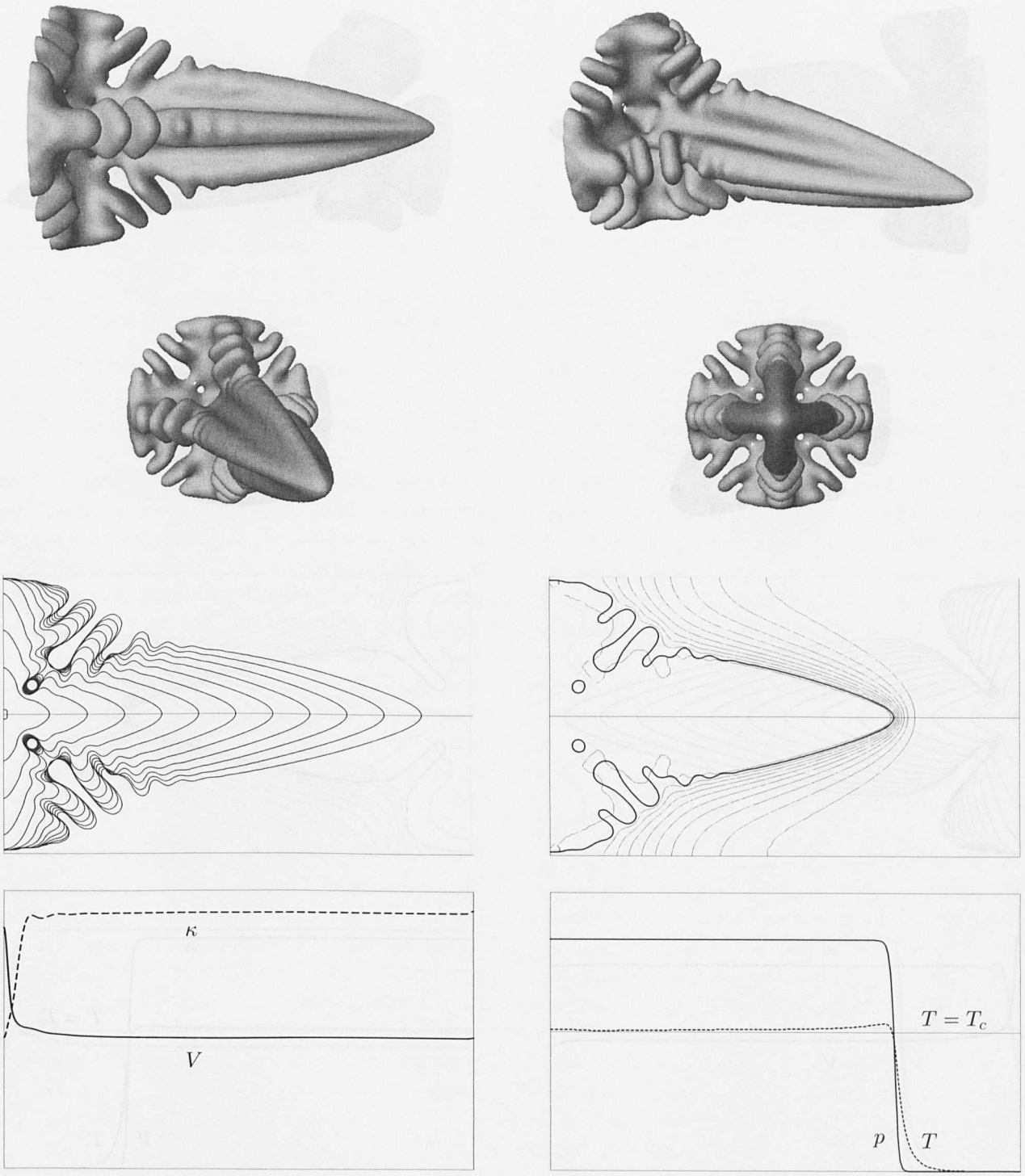

FIGURE 8. Simulation for $\delta = 0.5$. The arrangement is the same as in Figure 4.

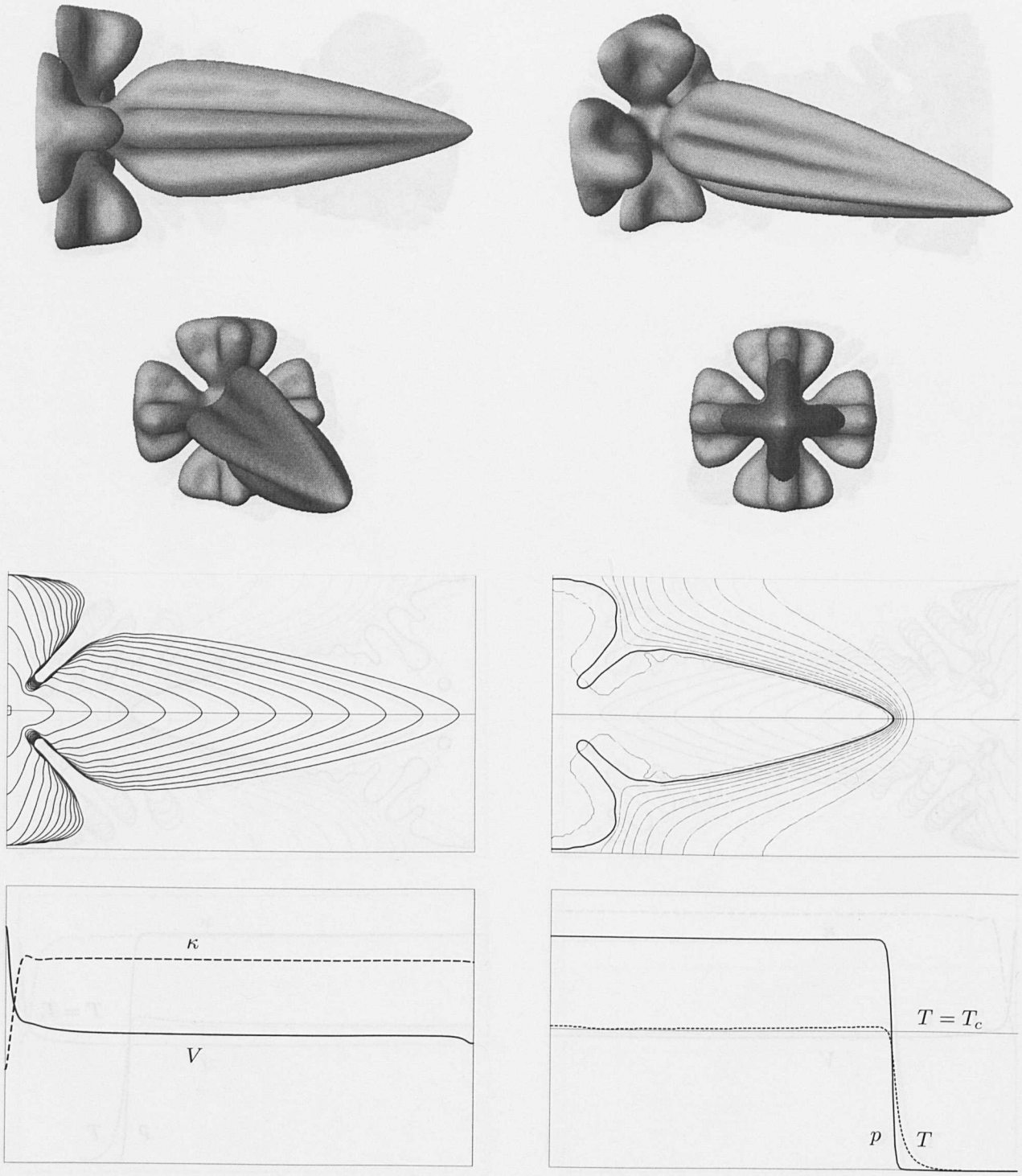

FIGURE 9. Simulation for $\delta = 0.8$. The arrangement is the same as in Figure 4.

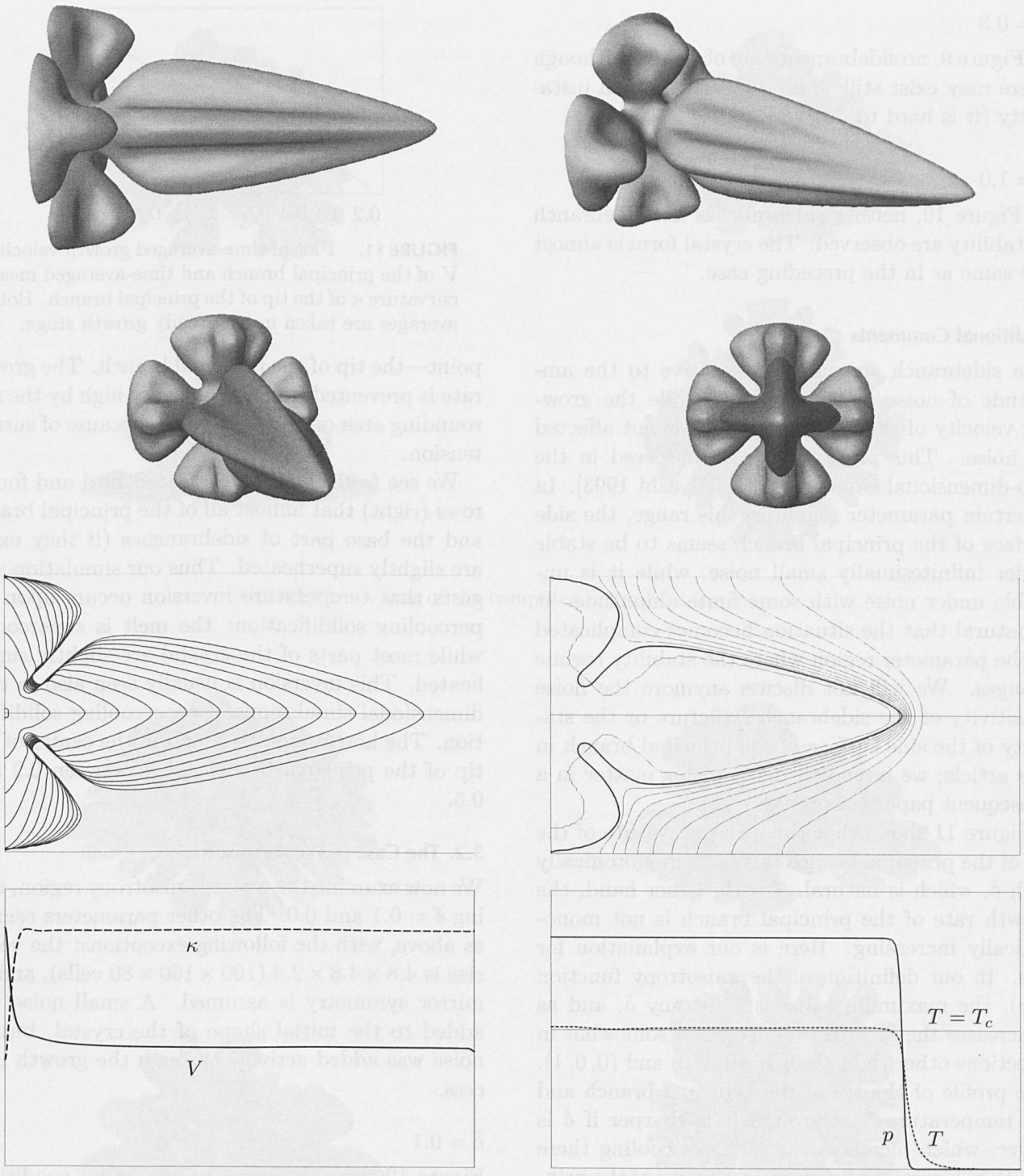

FIGURE 10. Simulation for $\delta = 1.0$. The arrangement is the same as in Figure 4.

$\delta = 0.8$

In Figure 9, no sidebranches are observed, although there may exist still some slight sidebranch instability (it is hard to tell).

$\delta = 1.0$

In Figure 10, neither sidebranches nor sidebranch instability are observed. The crystal form is almost the same as in the preceding case.

Additional Comments

The sidebranch structure is sensitive to the amplitude of noise when $\delta \geq 0.4$, while the growing velocity of the principal branch is not affected by noise. This property is also observed in the two-dimensional simulations [Kobayashi 1993]. In a certain parameter region in this range, the side surface of the principal branch seems to be stable under infinitesimally small noise, while it is unstable under noise with some finite amplitude. It is natural that the situation becomes complicated in the parameter region where the stability regime changes. We will not discuss anymore the noise sensitivity of the sidebranch structure or the stability of the side surface of the principal branch in this article; we intend to take up this matter in a subsequent paper (in preparation).

Figure 11 shows that the mean curvature of the tip of the principal branch increases monotonically with δ, which is natural. On the other hand, the growth rate of the principal branch is not monotonically increasing. Here is our explanation for this. In our definition of the anisotropy function $\sigma(v)$, the maximum value is 1 for any δ, and as δ increases the growth rate decreases somewhat in directions other than $(1,0,0)$, $(0,1,0)$ and $(0,0,1)$. The profile of the tip of the principal branch and the temperature field around it is sharper if δ is larger, which increases the effective cooling there and thus increases the growing velocity of the principal branch. That is why the growth rate increases for δ between 0.2 and 0.5. If δ increases more, the growth rate decreases even faster except for one

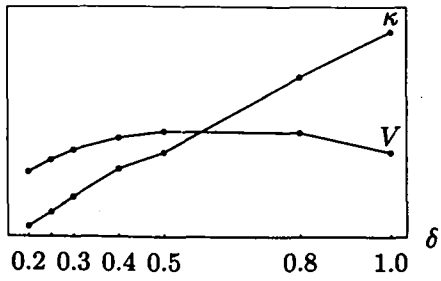

FIGURE 11. Plot of time-averaged growth velocity V of the principal branch and time-averaged mean curvature κ of the tip of the principal branch. Both averages are taken in the steady growth stage.

point—the tip of the principal branch. The growth rate is prevented from getting very high by the surrounding area on the tip surface, because of surface tension.

We see from the graphs on the third and fourth rows (right) that almost all of the principal branch and the base part of sidebranches (if they exist) are slightly superheated. Thus our simulation suggests that temperature inversion occurs upon supercooling solidification: the melt is supercooled while most parts of the crystal are slightly superheated. This inversion is usually seen also in two-dimensional simulations of supercooling solidification. The hottest spot is found in the center of the tip of the principal branch for δ between 0.2 and 0.5.

3.2. The Case of Weak Anisotropy

We now examine the weaker anisotropy region, taking $\delta = 0.1$ and 0.0. The other parameters remain as above, with the following exceptions: the vessel size is $4.8 \times 4.8 \times 2.4$ ($160 \times 160 \times 80$ cells), and no mirror symmetry is assumed. A small noise was added to the initial shape of the crystal, but no noise was added actively through the growth process.

$\delta = 0.1$

Figure 12 shows a crystal grown under conditions of weak anisotropy. Its shape is intermediate between those of the previous section and the one shown in Figure 13. We can observe the special

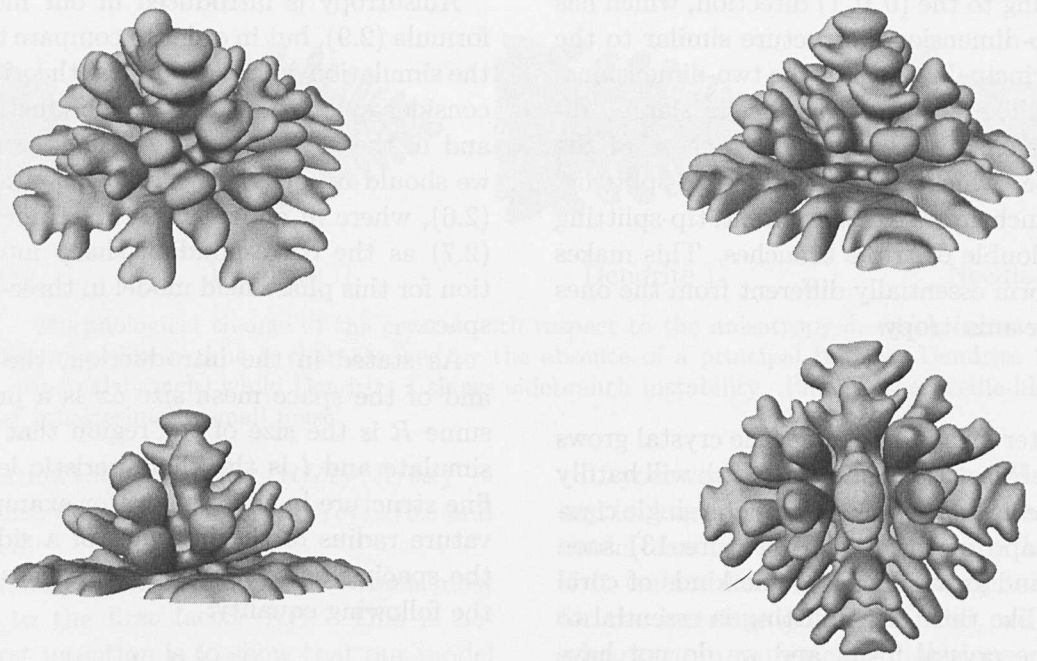

FIGURE 12. Views of the computed crystal for $\delta = 0.1$.

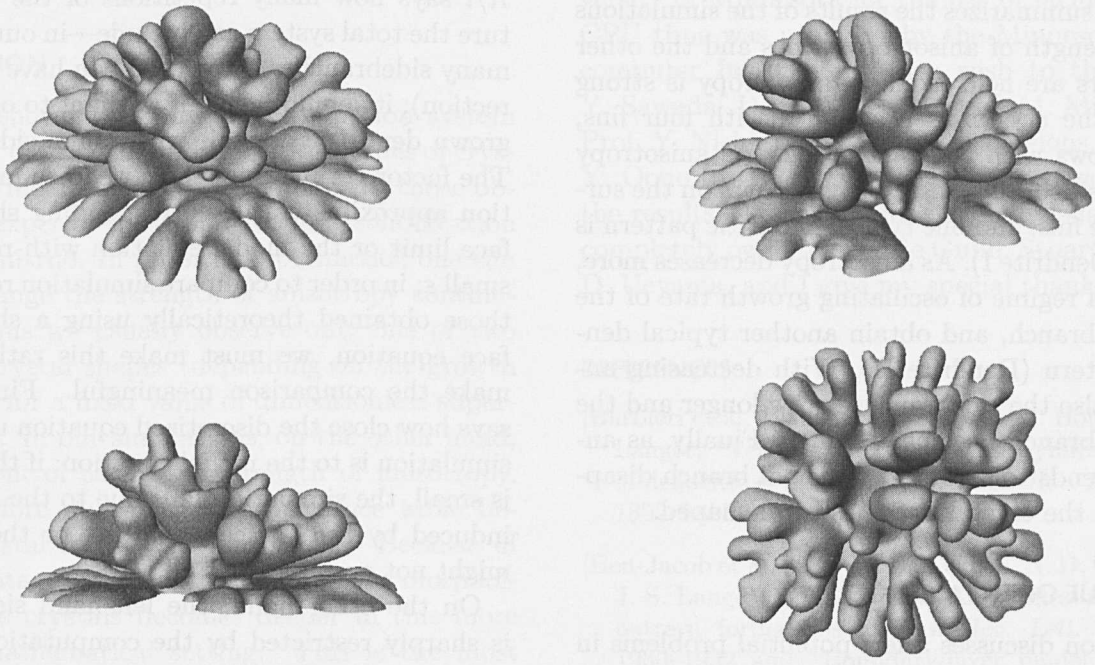

FIGURE 13. Views of the computed crystal for $\delta = 0$.

branch growing to the $(0, 0, 1)$ direction, which has almost a two-dimensional structure similar to the oscillating principal branch in the two-dimensional simulations. The branches growing in slanted directions have a similar structure to those of the isotropic case, which are formed by tip-splitting. Once the branch grows to some extent, tip-splitting occurs into double or triple branches. This makes the crystal form essentially different from the ones with stronger anisotropy.

$\delta = 0.0$

This parameter means, of course, the crystal grows in a completely isotropic manner, which will hardly happen in the usual growth process of a single crystal. The shape of the crystal (Figure 13) soon destabilizes and grows weird—some kinds of coral have shapes like this. Tip-splitting is essential to making of the crystal form, and we do not have a special branch in any sense. The branches are thicker than the ones in Figure 12.

3.3. Summary

Figure 14 summarizes the results of the simulations as the strength of anisotropy varies and the other parameters are held fixed. If anisotropy is strong enough, the crystal is needle-like with four fins, and it grows with constant speed. As anisotropy weakens, sidebranch instability appears on the surface of the fins, and one typical dendritic pattern is formed (Dendrite I). As anisotropy decreases more, we enter a regime of oscillating growth rate of the principal branch, and obtain another typical dendritic pattern (Dendrite II). With decreasing anisotropy also the sidebranches grow longer and the principal branch becomes thinner. Finally, as anisotropy tends to zero, the principal branch disappears and the crystal becomes coral-shaped.

4. CRITIQUE OF THE METHOD

This section discusses a few potential problems in the modeling and simulations presented in this article (see also the beginning of Section 3).

Anisotropy is introduced in our model via the formula (2.9), but in order to compare the results of the simulation with the physical theories we should consider anisotropy both in the kinetic coefficient and in the surface energy. Thus, as a next step, we should use for our interface equation Equation (2.6), where m depends on the temperature, with (2.7) as the corresponding sharp interface equation for this phase field model in three-dimensional space.

As stated in the introduction, the choice of ε and of the space mesh size δx is a problem. Assume R is the size of the region that we want to simulate and l is the characteristic length of the fine structure in the system (for example, the curvature radius of the interface of a sidebranch, or the spacing between the sidebranches). Consider the following equality:

$$\frac{R}{\delta x} = \frac{R}{l} \cdot \frac{l}{\varepsilon} \cdot \frac{\varepsilon}{\delta x} \tag{4.1}$$

Each of the quotients in the right-hand side needs to be relatively large for good results. The factor R/l says how many repetitions of the fine structure the total system can include—in our case, how many sidebranches the crystal can have (in one direction); it should be big if we want to obtain well-grown dendritic crystals with many sidebranches. The factor l/ε measures how well the model equation approximates the corresponding sharp interface limit or the model equation with realistically small ε; in order to compare simulation results with those obtained theoretically using a sharp interface equation, we must make this ratio large to make the comparison meaningful. Finally, $\varepsilon/\delta x$ says how close the discretized equation used in our simulation is to the model equation; if this number is small, the simulation fails due to the anisotropy induced by the lattice structure, or the interface might not even move at all.

On the other hand, the left-hand side of (4.1) is sharply restricted by the computational power and memory available. In three dimensions, the necessary memory size is proportional to $(R/\delta x)^3$,

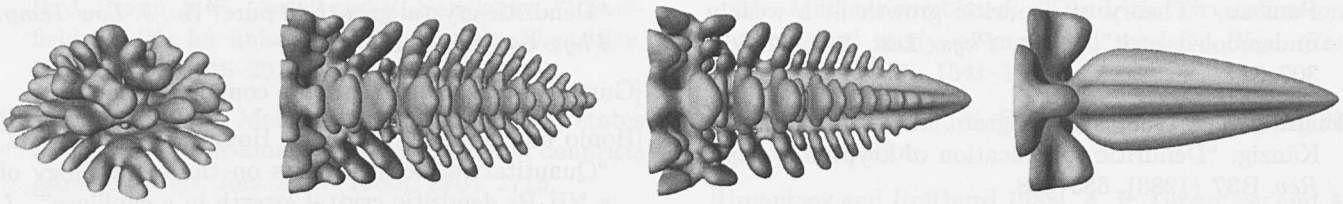

Coral-like Dendrite II Dendrite I Needle-like

FIGURE 14. Morphological change of the crystal with respect to the anisotropy δ, which increases from left to right. The coral-like regime is characterized by the absence of a principal branch. Dendrite II shows an oscillating principal branch, while Dendrite I shows sidebranch instability. Finally, the needle-like regime is stable under infinitesimally small noise.

and computation time is of order $(R/\delta t)\cdot(R/\delta x)^3 \sim (R^4/\delta x^5)$, since $\delta t \sim \delta x^2$ as long as $\tau/\delta t$, $\varepsilon/\delta x$ and τ/ε^2 are fixed.

In the simulations of Section 3, we attach most importance to the first factor R/l. This is because our first intention is to show that our model can simulate realistic three-dimensional dendrites. Such restrictions will be gradually eased by the continual improvement in computers, so at this point we can be optimistic.

CONCLUSION

We have shown that the model equation system (2.10) and (2.11) can produce various types of crystal forms, including ones very similar to those observed in experiments of supercooling solidification of succinonitrile. In physical experiments, one can hardly change the strength of anisotropy continuously. Thus we usually observe only one or two types of crystal shapes (depending on the growth direction) for a fixed value of dimensionless supercooling Δ. In our simulations, on the other hand, we can control easily the strength of anisotropy, and therefore obtain a correspondence table between crystal forms and anisotropy. Because of this advantage, our understanding of the morphology of the crystals becomes deeper in this more general mathematical setting. This is the most important and useful point of the modeling and simulation approach presented here.

If you wear glasses, take them off for a minute and look around. You will get a feeling for how the model can capture the large-scale behavior even if it cannot keep track of fine detail. In return for the interface getting blurred, we have a great advantage in numerical simulations—simplicity.

ACKNOWLEDGMENTS

I wish to thank the Geometry Center at the University of Minnesota for the use of facilities. Cray CPU time was provided by the Minnesota Supercomputer Institute. I also wish to thank Prof. Y. Sawada, Dr. A. Tanaka, Prof. M. Mimura and Prof. Y. Nishiura for fruitful discussions, and Prof. Y. Oono for the Cray CPU time needed to check the results. The three-dimensional visualization is completely owed to Charlie Gunn, Stuart Levy and D. Ueyama, and I give my special thanks to them.

REFERENCES

[Barbieri et al. 1986] A. Barbieri, D. C. Hong and J. S. Langer, "Velocity selection in the symmetric model of dendritic crystal growth", *Phys. Rev.* A**35** (1986), 1802–1808.

[Ben-Jacob et al. 1984] E. Ben-Jacob, N. D. Goldenfeld, J. S. Langer and G. Schön, "Dynamics of interfacial pattern formations", *Phys. Rev. Lett.* **51** (1983), 1930–1932 and "Boundary-layer model of pattern formation in solidification", *Phys. Rev.* A**29** (1984), 330–340.

[Ben Amar and Pomeau 1986] M. Ben Amar and Y. Pomeau, "Theory of dendritic growth in a weakly undercooled melt", *Euro. Phys. Lett.* **2**(4) (1986), 307–314.

[Bilgram et al. 1988] J. H. Bilgram, M. Fireman and W. Känzig, "Dendritic solidification of krypton", *Phys. Rev.* **B37** (1988), 685–688.

[Brower et al. 1983] R. C. Brower, D. A. Kessler, J. Koplik and H. Levine, "Geometrical approach to moving-interface dynamics", *Phys. Rev. Lett.* **51** (1983), 1111–1114.

[Caginalp 1986] G. Caginalp, "An analysis of a phase field model of a free boundary", *Arch. Rat. Mech. Anal.* **92** (1986), 205–245.

[Caginalp 1989] G. Caginalp, "Stefan and Hele–Shaw type models as asymptotic limits of the phase-field equations", *Phys. Rev.* **A39** (1989), 5887–5896.

[Caginalp and Nishiura 1991] G. Caginalp and Y. Nishiura, "The existence of travelling waves for phase field equations and convergence to sharp interface models in the singular limit", *Quart. Appl. Math.* **49** (1991), 147–162.

[Caroli et al. 1986] B. Caroli, C. Caroli, B. Roulet and J. S. Langer, "Solvability condition for needle crystals at large undercooling in a nonlocal models of solidification", *Phys. Rev.* **A33** (1986), 442–452.

[Carr and Pego 1989] J. Carr and R. L. Pego, "Metastable patterns in solutions of $u_t = \epsilon^2 u_{xx} - f(u)$", *Comm. Pure Appl. Math.* **42** (1989), 523–576.

[Collins and Levine 1985] J. B. Collins and H. Levine, "Diffuse interface model of diffusion-limited crystal growth", *Phys. Rev.* **B31** (1985), 6119–6122.

[Dougherty et al. 1987] A. Dougherty, P. D. Kaplan and J. P. Gollub, "Development of side branching in dendritic crystal growth", *Phys. Rev. Lett.* **58** (1987), 1652–1655.

[Fife and McLeod 1977] P. C. Fife and J. B. McLeod, "The approach of solutions of nonlinear diffusion equations to travelling front solutions", *Arch. Rat. Mech. Anal.* **65** (1977), 335–361.

[Fix 1983] G. Fix, "Phase field models for free boundary problems", pp. 580–589 in *Free Boundary Problems*, edited by A. Fasano and M. Primicero, Pitman, New York, 1983.

[Franck and Jung 1986] J. P. Franck and J. Jung, "Dendritic crystal growth in pure ^{4}He, *J. Low Temp. Phys.* **64** (1986), 165–186.

[Gurtin] M. E. Gurtin, private communication.

[Honjo and Sawada 1982] H. Honjo and Y. Sawada, "Quantitative measurements on the morphology of a NH_4Br dendritic crystal growth in a capillary", *J. Cryst. Growth* **58** (1982), 297–303.

[Huang and Glicksman 1981] S. -C. Huang and M. E. Glicksman, "Fundamentals of dendritic solidification, I: Steady-state tip growth" and "II: Development of sidebranch structure", *Acta. Metal.* **29** (1981), 701–716 and 717–734.

[Kessler and Levine 1987] D. A. Kessler and H. Levine, "Stability of dendritic crystals", *Phys. Rev. Lett.* **57** (1987), 3069–3072.

[Kessler et al. 1986] D. A. Kessler, J. Koplik and H. Levine, "Steady-state dendritic crystal growth", *Phys. Rev.* **A33** (1986), 3352–3357.

[Kobayashi 1987] R. Kobayashi, "Dynamics of interfaces in systems of reaction diffusion", *RIMS Kokyuroku* **614** (1987), 39–54 (in Japanese).

[Kobayashi 1991] R. Kobayashi, "Modeling and simulations of crystal growth", pp. 24–25 in *Computational Optimal Geometries*, edited by J. E. Taylor, Amer. Math. Soc., Providence, 1991 (includes videotape footage).

[Kobayashi 1992] R. Kobayashi, "Simulations of three dimensional dendrites", pp. 121–128 in *Pattern Formation in Complex Dissipative Systems*, edited by S. Kai, World Scientific, Singapore and Philadelphia, 1992.

[Kobayashi 1993] R. Kobayashi, "Modeling and numerical simulations of dendritic crystal growth", *Physica* **D63** (1993), 410–423.

[Langer 1986] J. S. Langer, "Models of pattern formation in first-order phase transitions", pp. 165–186 in *Directions in Condensed Matter Physics*, edited by G. Grinstein and G. Mazenko, World Scientific, Singapore and Philadelphia, 1986.

[Maurer et al. 1989] J. Maurer, P. Boissou, B. Perrin and P. Tabeling, "Faceted dendrites in the growth of NH_4Br crystals", *Euro. Phys. Lett.* **8**(1) (1989), 67–72.

[McFadden et al. 1993] G. B. McFadden, A. A. Wheeler, R. J. Braun, S. R. Coriell and R. F. Sekerka, "Phase-field models for anisotropic interfaces", *Phys. Rev.* **E48** (1993), 2016–2024.

[Meiron 1986] D. I. Meiron, "Selection of steady states in the two-dimensional symmetric model of dendritic growth", *Phys. Rev.* **A33** (1986), 2704–2715.

[Mottoni and Schatzman 1990] P. de Mottoni and M. Schatzman, "Development of interfaces in R^N", *Proc. Royal Soc. Edin.* **116A** (1990), 207–220.

[Pelcé and Pomeau 1986] P. Pelcé and Y. Pomeau, "Dendrites in the small undercooling limit", *Studies in Appl. Math.* **74** (1986), 245–258.

[Penrose and Fife 1990] O. Penrose and P. C. Fife, "Thermodynamically consistent models of phase-field type for the kinetics of phase transitions", *Physica* **D43** (1990), 44–62.

[Saito et al. 1987] Y. Saito, G. Goldbeck-Wood and H. Müller-Krumbhaar, "Dendritic Crystalization: Numerical study of one-sided model", *Phys. Rev. Lett.* **58** (1987), 1541–1543.

[Sawada and Inoue] Y. Sawada and T. Inoue, private communication.

[Umantsev and Roĭtburd 1988] A. R. Umantsev and A. L. Roĭtburd, "Nonisothermal relaxation in a nonlocal medium", *Sov. Phys. Solid State* **30** (1988), 651–655.

[Wheeler et al. 1993] A. A. Wheeler, B. T. Murray and R. J. Schaefer, "Computation of dendrites using a phase field model", *Physica* **D66** (1993), 243–262.

[Yokoyama and Kuroda 1990] Y. Yokoyama and T. Kuroda, "Pattern formation in growth of snow crystals occurring in the surface kinetic process and the diffusion process", *Phys. Rev.* **A41** (1990), 2038–2049.

Ryo Kobayashi, Department of Applied Mathematics and Informatics, Ryukoku University, Seta, Ohtsu 520-22, Japan (ryo@rins.ryukoku.ac.jp)

Received September 29, 1993; accepted in revised form June 16, 1994